

# Reconstructing past changes in atmospheric processes at Europe's northernmost concentric bog: 6000 years of change in elemental chemistry at the Sellevollmyra Bog (Andøya, Arctic Norway)

Jennyann Andersson



Department of Geological Sciences  
Degree project in Geochemistry 15 hp  
Earth Science Programme 180 hp  
Spring Term 2025  
Supervisor: Malin Kylander



Stockholms  
universitet

## **Abstract**

Ombrotrophic bogs serve as excellent archives of past atmospheric conditions as, by definition, they are only supplied by atmospheric inputs. The generally slow accumulation rates of peat enable records covering thousands of years in sequences of just a few meters providing a relatively easily acquired and, thanks to the high organic content, age dated, terrestrial record. In comparison to ice cores, peat bogs show greater global distribution. The purpose of the present study is to expand on an earlier study from Sellevollmyra, a coastal bog on the island of Andøya in Arctic Norway, which focused largely on the organic aspects of the bog. For this study, we have used X-Ray Fluorescence (XRF) and a mercury analyzer to investigate the inorganic geochemical properties of the bog to further build on our understanding of the elemental behaviors in the bog, its formation, pollution at a high-latitude arctic site, and to reconstruct past mineral dust fluctuations. Findings include Ca, Mn, and Fe unsurprisingly acting mobile, and using these it was concluded that the bog formed through soil paludification and that the fen bog transition happened at around 354-323 cm. A generally low amount of pollution was found, and Hg was determined to act mobile due to the presence of Cl. However, the overall focus was on identifying past dust events using the conservative elements Al, Si, K, and Ti. The eleven dust events found were at depths of 359-358 cm, 259-253 cm, 234-233 cm, 214-213 cm, 204-183 cm, 159-148 cm, 139-138 cm, 129-128 cm, 109-108 cm, 89-83 cm, and 54-48 cm in the composite sequence. This agrees with available regional records and can largely be linked to findings in the Vorren et al. (2007) study.

## 1 Introduction and background

Peat bogs have been used for atmospheric reconstructions since the turn of the 20<sup>th</sup> century (Blackford, 2000). The slow accumulation rates of peat bogs provide archives potentially covering one or two decades in just a centimeter of material. Ombrotrophic peat bogs are by definition only supplied by atmospheric inputs and are therefore often used for reconstructing past and present atmospheric deposition (Hansson et al., 2015). The true importance of peat as an archive of past atmospheric conditions becomes clear when considering other potential archives. Peat bogs and continental ice sheets are the only two archives which exclusively record atmospheric signals, and of the two, peat bogs have a much wider global distribution and can be found both in regions influenced by human activity and in remote areas (Martínez Cortizas et al., 2002). Previous studies have found a suite of elements that are considered mobile in peat bogs, namely Ca, Fe, Mn, Mg, and Sr (Boyer et al., 2018; Damman, 1978; Gorham and Janssens, 2005).

Peatland formation generally starts through one of two processes: terrestrialization of a lake or soil paludification (Schaffhauser et al., 2017). Of the two, paludification is the most common, a process of accumulation of organic matter over time, starting on a terrestrial surface (Lavoie, 2005; Schaffhauser et al., 2017). It is believed to be caused by increasing moisture in the soil and colonization of *Sphagnum*. Schaffhauser et al. (2017) described that paludification is generally a two-stage process, the first stage being minerotrophic fen followed by a transition to an ombrotrophic bog. Relatively high ash, Ca and Fe, amongst enrichment in a few other elements, signals minerotrophic fen conditions, while a lowering of these suggest a transition into ombrotrophy (Sjöström et al., 2022). Which of the two initiation processes that will act upon peatland formation is dependent on many different factors, including climate and hydrology (Schaffhauser et al., 2017). Whether the result of said processes is a fen or a bog is largely controlled by the water availability and composition of the soligenous water.

Since the 1970s, peat bogs have been used with increasing frequency to reconstruct historical pollution events and trends, both locally and globally (Hansson et al., 2015). Understanding past pollution deposition can give important insight into the potential impacts of contemporary pollution (Jones and Hao, 1993). Human activities have significantly impacted atmospheric emissions of a broad range of heavy metals, making it important to study both the natural background values and the actual emission levels of these with a view to setting reasonable environmental targets (De Vleeschouwer et al., 2010).

Heavy metals are known to have negative effects on human health (Odukoya et al., 2000) and the environment (Timothy and Williams, 2019). In an article evaluating pollution levels and health risks of heavy metals near Cu mining sites, Chen et al. (2022) writes that heavy metals in soil, including Cu and Pb, may damage the functions of the stomach, kidney, and cardiovascular tissues, amongst other organs, and can cause cancer. Lead in particular is one of the most toxic metals on Earth and it accumulates in organisms and the environment due to its non-biodegradable properties (Mandal et al., 2022; Meena et al., 2019). Zinc, while an essential micronutrient for plant growth, can also cause harm when found in excess (Van et al., 2024). Accumulation of Zn can reduce soil fertility and potentially become toxic for plants and microorganisms. As for Hg, there have been no biological benefits found, meaning all forms have been classed as toxic (Hylander and Goodsite, 2006). The main effected organ of Hg-poisoning is the brain where the metal destroys neurons in the visual cortex and cerebellar granule cells (Kao et al., 2004).

Atmospheric dust plays a role in the climate system in various ways, providing nutrients to soil and marine systems, interacting with incoming solar radiation, impacting cloud formation processes through providing cloud condensation nuclei, and causing respiratory diseases (Albani et al., 2015; Knippertz and Stuut, 2014; Kylander et al., 2016; Kylander et al., 2018). Not all elements can be used as indicators of atmospheric conditions since a requirement is that they remain immobile post deposition (Novak and Pacherova, 2008). Mobile elements affected by water transport are therefore not a reliable source of past atmospheric depositions (Novak et al., 2011). Since about three quarters of the estimated total amount of dust deposited each year ends up in terrestrial settings it is important to expand the spatial coverage of archives of global dust deposition (Kylander et al., 2016). At the time of the present thesis, no other studies have been made on mineral dust in northern Norway.

Previous studies have used lithogenic elements as proxies for dust deposition in peat bogs (Martínez Cortizas et al., 2019) and records of grain size and sand accumulation rates (SARs) have been used as indicators of past increased storminess (Sjögren, 2009; Vandel et al., 2019). With increased grain size and amount of dust we would generally assume either drier conditions or changes in wind activity, including strengths and directions, but things like vegetation may also affect dust concentrations. Sjögren (2009), who studied SARs in northern Norway over the past 3000 years, mentions that variations in dust may largely coincide with changes in ocean currents, which in turn are affected by winds and precipitation. In other words, storminess may bring increased amounts of dust and affect ocean currents. For this study,

lithogenic elements are investigated and used as proxies for past dust events and in turn, climatic conditions and storminess.

### **1.1 Aim**

The aim of this thesis is to identify and reconstruct past atmospheric processes in Europe's northernmost concentric bog Sellevollmyra on the island of Andøya in the high Norwegian Arctic. A previous study at this site focused largely on establishing a high-resolution stratigraphy of the sequence, quantifying paleovegetation, identifying tephra and specific volcanic eruptions, and degree of humification (Vorren et al., 2007). The purpose of the present thesis is to assess the inorganic geochemical properties of the bog and expand on the Vorren et al. (2007) study. The specific objectives are to (i) understand the elemental behavior in the bog, (ii) build on our understanding of the bog formation, (iii) investigate anthropogenic pollution at a high latitude, Arctic site, and (iv) explore past mineral dust variations.

### **1.2 Site description**

Sellevollmyra is Europe's northernmost concentric bog, located on the island Andøya in the Vesterålen archipelago, northern Norway (Vorren et al., 2007). It covers an area of just over 1 km<sup>2</sup> with the concentric pattern center at approximately 69°06'11"N and 15°55'25"E (fig. 1). Vorren et al. (2007) described it as an asymmetric concentric bog where the pattern is formed by pools, hollows, and string hummocks. Presently, the site is situated 14 m a.s.l.

The bedrock in the Vesterålen area is dominated by Precambrian rocks (Olesen et al., 2002). There are gabbros, Archean gneisses, as well as some transscandinavian igneous belt (TIB) granitoids, ~1.86-1.76 Ga. With the retreat of the last ice sheet the area experienced deep erosion, but not a lot of sedimentation (Olsen et al., 2013). The area is characterized by weathered bedrock, either completely exposed or with a thin, loose sediment cover, and is part of a discontinuous blockfield/field of weathered material.

Mountains reaching 500-1000 m a.s.l. near the coast of the Lofoten-Vesterålen archipelago act as barriers to the cool and moist Atlantic air masses (Kirchhefer, 2001). This leads to the alpine areas receiving up to 2500 mm of precipitation per year, and the coastal regions around 1000 mm annually. Coastal summer temperatures reach about 11°C while the inner part of the archipelago sees temperatures of 12-12,5°C at sea level. Using dendroclimatology, Kirchhefer (2001) reconstructed July-August temperatures of Andenes, just

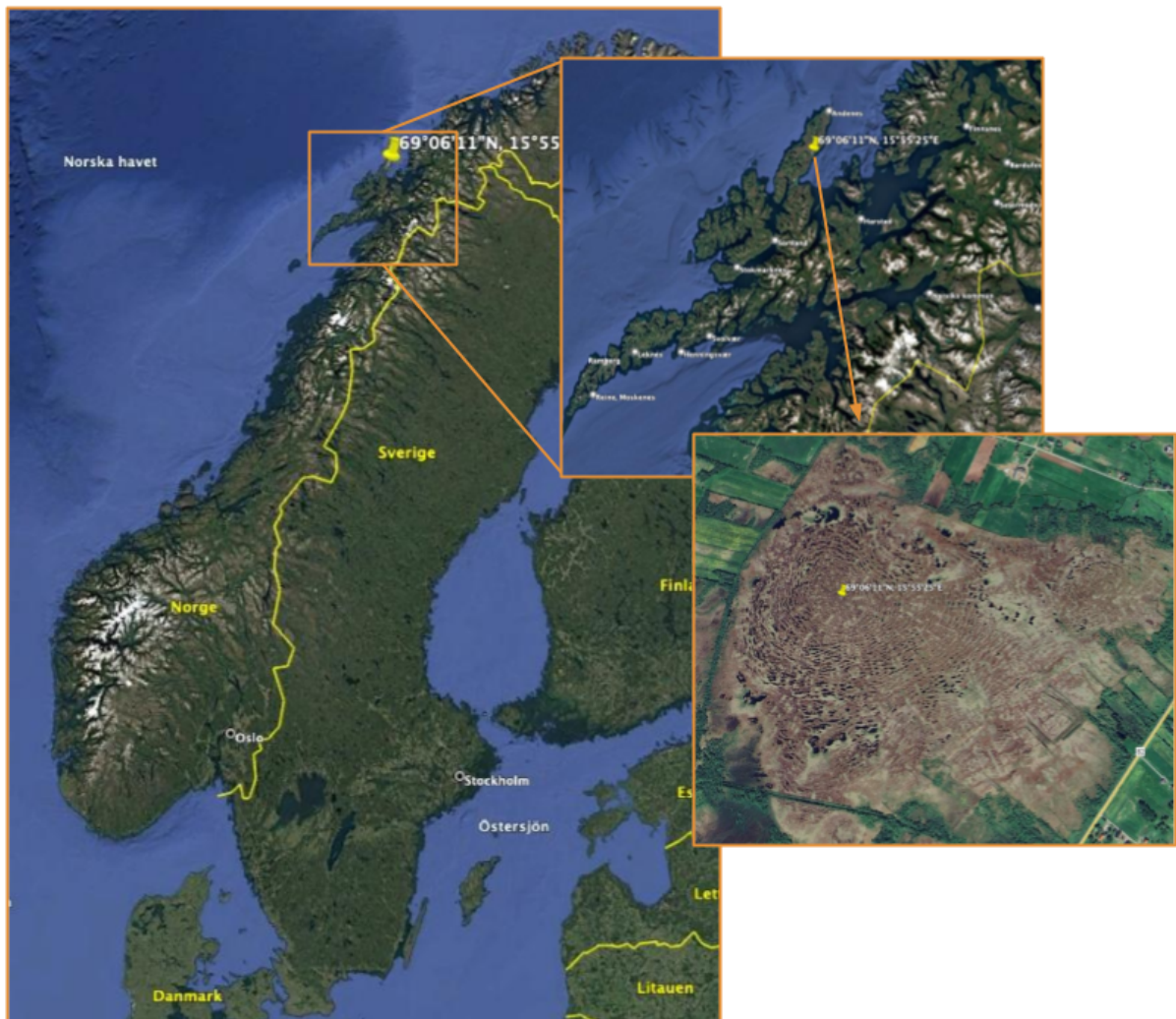


Fig. 1 – The study site Sellevollmyra bog located at 69°06'11"N and 15°55'25"E.

north of Andøya, back to 1550 CE. Temperatures seem to have stayed around 11°C for the last ca 450 years, but with a slight upward trend from 1900 CE onward, following a short period of low temperatures. At Forfjorddalen, a valley a bit south of Andøya, the reconstruction reached back to 1350 CE. Here, summer temperatures seem to have been even more stable around 11°C.

## 2 Method and materials

### 2.1 Coring

The Sellevollmyra sequence was retrieved in June of 2024. Coring was carried out in two adjacent parallel holes near the center of the bog using a Russian corer measuring 7.5 cm in diameter and 1 m in length. The cores overlapped by ca 25 cm. They were wrapped in plastic, placed in PVC liners and transported to the laboratory where they were stored at 8°C until further laboratory work was made.

## **2.2 CT-scanning and core alignment**

The six cores were CT-scanned to acquire wet density variations. This data was then used to align the cores and generate a composite sequence of 438 cm. The convention for aligning peat cores has been to use the dry bulk density of discrete samples while the Sellevollmyra cores were scanned wet in order to save time.

## **2.3 Subsampling**

Subsampling of the sequence was done using a stainless-steel knife to cut 1 cm slices approximately every fifth centimeter. Due to the small amount of material in the topmost part of the sequence, the first subsample had to be 5 cm thick and was taken in Core 1 at 22-27 cm where there was enough material to sample. After the second sample, which had to be 2 cm thick at 34-36 cm, the regular 1 cm subsampling commenced. The subsamples were put in individual bags labelled with both the core number (C1-C6) and the depth within that core from which they were cut. Rubber gloves were used when handling the samples to avoid contamination. In total 82 slices were cut.

## **2.4 Freeze-drying**

The subsamples were frozen overnight in preparation for being freeze-dried. The frozen samples were then arranged on plates with their bags open. To ensure that the samples would still be completely frozen they were then put back in the freezer for 20 min before the sample filled plates were put into the Scanvac CoolSafe freeze drier. They were left to dry for 4-5 days.

## **2.5 Milling**

The samples were milled to a fine powder and homogenized using a Lab Wizz 320 Micro Ball Mill in preparation for the Hg and X-Ray Fluorescence (XRF) analyses. The time was set to 3 min and 30 s and the number of strokes was set to 40. When a sample was done, it was checked visually for texture and milled again if too coarse/grassy.

## **2.6 Hg-analyses**

To measure the concentration of Hg in each of the samples, the DMA-80 evo, a direct mercury analyzer, was used. For each measurement, 30-40 mg of peat was weighed out on a Sartorius high precision scale.

### *2.6.1 Lower detection limit*

The lower detection limit was found using empty containers (boats) at the start and end of each day (two days were used), as well as after approximately every tenth boat. For the empty boats, the weight was set to 1 g so that the total measured Hg would equal the concentration in  $\mu\text{g kg}^{-1}$ . What these measurements show is the potential residual Hg in the analyzer which marks the lower detection limit. For measurements below this limit, it cannot be said for certain that a sample contains any Hg as it could be residuals from other samples.

### *2.6.2 Reference material*

To calculate the standard deviation (STD) and coefficient of variation (CV) of the analyzer, the reference material NIMT/UOE/FM/001 (Yafa et al., 2004) was used. A total of ten measurements were made on the material and the STD came out to  $\sim 3.8 \mu\text{g kg}^{-1}$  and the CV came out to  $\sim 2.07\%$ . This indicates that the instrument is precise. However, the mean Hg concentration came to  $\sim 183 \mu\text{g kg}^{-1}$  while the certified value was  $169 \mu\text{g kg}^{-1}$ . This points to the instrument having a positive bias. To somewhat account for this bias, 1 STD was subtracted from each of the measurements.

## **2.7 XRF**

XRF analyses were made using a WDXRF (wavelength dispersive) analyzer at Umeå University. However, before all samples had been analyzed there were some technical difficulties, so an EDXRF (energy dispersive) analyzer had to be used for a portion of the bottommost core. With both instruments, 500 mg of peat was weighed into 20 mm cups that had been prepared with a thin plastic bottom. Caution was taken to not touch the plastic at any point as that would affect the results.

XRF spectrometry, or X-ray fluorescence spectrometry, is a technique used to measure the bulk elemental concentrations in materials (Johnson and King, 1987). The materials are exposed to primary X-ray radiation which excites the atoms, causing ionization (Johnson and Kings, 1987; Potts, 1987). When the atoms then de-excite and the electrons rearrange, fluorescent X-rays are emitted. Each element has its own characteristic fluorescent X-ray energy and can therefore be identified upon detection (Johnson and King, 1987). The difference between EDXRF and WDXRF is in the detector system. Energy dispersive XRF measures all of the fluorescent X-rays simultaneously and gives results in real time (Johnson and Kings, 1987; Potts, 1987). Wavelength dispersive XRF rather utilizes crystalline materials with the capability of diffracting X-rays based on their wavelengths to split up the element

characteristic X-rays (Potts, 1987). The detector then measures the X-rays separately to analyze the concentration of the various elements. EDXRF has more severe line overlaps than WDXRF and is less sensitive for the light elements (Johnson and King, 1987).

### *2.7.1 WDXRF*

The elemental data from the top of the sequence down to sample C5 72-73 (334 cm) was made using the Bruker S8 Tiger ECO, a WDXRF spectrometer. About every 20<sup>th</sup> sample was replicated and three reference materials were run sporadically. One was the Yafa et al. (2004) NIMT/UOE/FM/001 reference material and the other two were in-house reference materials. Before the technical difficulties occurred, this resulted in the two in-house reference materials being run four times each, the Yafa et al. (2004) reference was run one time, and two sample replicates were made. The S8 Tiger measured Na, Mg, Al, Si, P, S, Cl, K, Ca, Ti, Mn, Fe, Ni, Cu, Zn, As, Br, Rb, Sr, Ba, and Pb.

### *2.7.2 EDXRF*

For the rest of the samples, C5 77-78 to C6 97-98 (338-438 cm), the Bruker S1 Titan, an EDXRF spectrometer, was used. The same reference materials were analyzed once at the start and once at the end, after the C6 97-98 sample. For the EDXRF samples, two replicates were made. The S1 Titan measures all elements that it detects, meaning it gave data for some additional elements which were not analyzed with the S8 Tiger. The S1 Titan gave outputs for Mg, Al, Si, P, S, Cl, K, Ca, Ti, V, Cr, Mn, Fe, Ni, Cu, Zn, As, Se, Br, Rb, Sr, Mo, Cd, Ba, Hg, and Pb. However, many of these ended up not being used due to all or most of the outputs coming out as “< LOD”, below limit of detection. These included Si, K, V, Ni, As, Se, Rb, Mo, Cd, Ba, and Hg.

The two instruments measured some elements differently from each other. To deal with this, seven samples from Core 5 that had been run in the S8 Tiger were also analyzed using the S1 Titan. Corrections were made by calculating the difference in percentage between the S8 Tiger and S1 Titan measurements and applying the multiplicative factor to the affected S1 Titan dataset.

## **2.8 Dry-ashing**

Dry-ashing was used to measure the inorganic material in each sample. Crucibles were placed in an oven at 105°C for a minimum of 4 h to ensure absence of water. These were then put into

an airtight cabinet and weighed once cooled sufficiently. Each crucible was numbered, and their weights were documented. The weighed crucibles were filled with peat samples. These were then put onto trays and placed into the 105°C oven, again for a minimum of 4 h to ensure removal of any excess moisture. The sample-filled crucibles were then weighed in the same way as the empty crucibles. These samples were then ashed in a Nabertherm high temperature furnace which was set to 500°C. After 4 h at 500°C, the oven was programmed to go back down to 105°C to ensure no water gain. The ashed samples were then weighed. Inorganic content (ash %) was calculated by dividing the weight of the ashed sample ((ashed peat + crucible) – crucible) by the weight of the dry peat ((dry peat + crucible) – crucible) and multiplying by 100.

### 3 Results

#### 3.1 XRF

For the presentation of the XRF results, the WDXRF and corrected EDXRF are treated as one dataset. Where the EDXRF failed to measure a certain element due to low concentrations, the graph will simply cut off after the WDXRF data. Negative outputs are treated as 0. Out of the 23 unique elements that were detected, nine elements, Na, S, P, Ni, As, Br, Rb, Ba, and Cr, will not be discussed further and therefore not be presented. For visualization and discussion, five periods were defined based on the general behavior of the elemental data. These are: Period I: 438-398 cm, Period II: 394-223 cm, Period III: 219-148 cm, Period IV: 144-73 cm, and Period V: 69-22 cm.

##### 3.1.1 Mobile elements: Ca, Mn, Fe, Sr and Mg

The mobile element concentrations are presented in fig. 2 along with the ash content. Calcium (mean  $0.23 \pm 0.04\%$ , range = 0.14-0.33%, n = 82), Mn (mean  $7.97 \pm 15.37$  ppm, range = 0-63.5 ppm, n = 82), and Fe (mean  $0.1 \pm 0.1\%$ , range = 0.03-0.36%, n = 82) all show similar curves and are also somewhat similar to the ash content. There is a general decrease in concentration from the oldest part of the sequence up to ca 273 cm, with two prominent dips at 399-398 cm and 359-358 cm. The Ca shows oscillations further up in the sequence, but the concentration is generally low. There is no Mn present above 333 cm and the Fe shows a very even, low concentration curve above ~258 cm. Both Sr (mean  $23.7 \pm 6.38$  ppm, range = 6.93-34 ppm, n = 82) and Mg (mean  $0.31 \pm 0.09\%$ , range = 0-0.48%, n = 82) are somewhat inverted in comparison

to the other mobile elements where they see generally lower values in the oldest ca 40 cm and higher values in the younger parts of the sequence. Both elements also show more dramatic variations when compared to the other mobile element graphs (fig. 2). The Sr vs Mg scatterplot (fig. 3) show correlations between the two as the points group around the same area when excluding the anomalous oldest part, Period I.

Scatterplots of the mobile elements Mn, Fe, Sr, and Mg in relation to Ca are seen in fig. 4, with period divisions. The three youngest periods show clear grouping in all of the plots, whereas the two oldest sections generally stray from the other points.

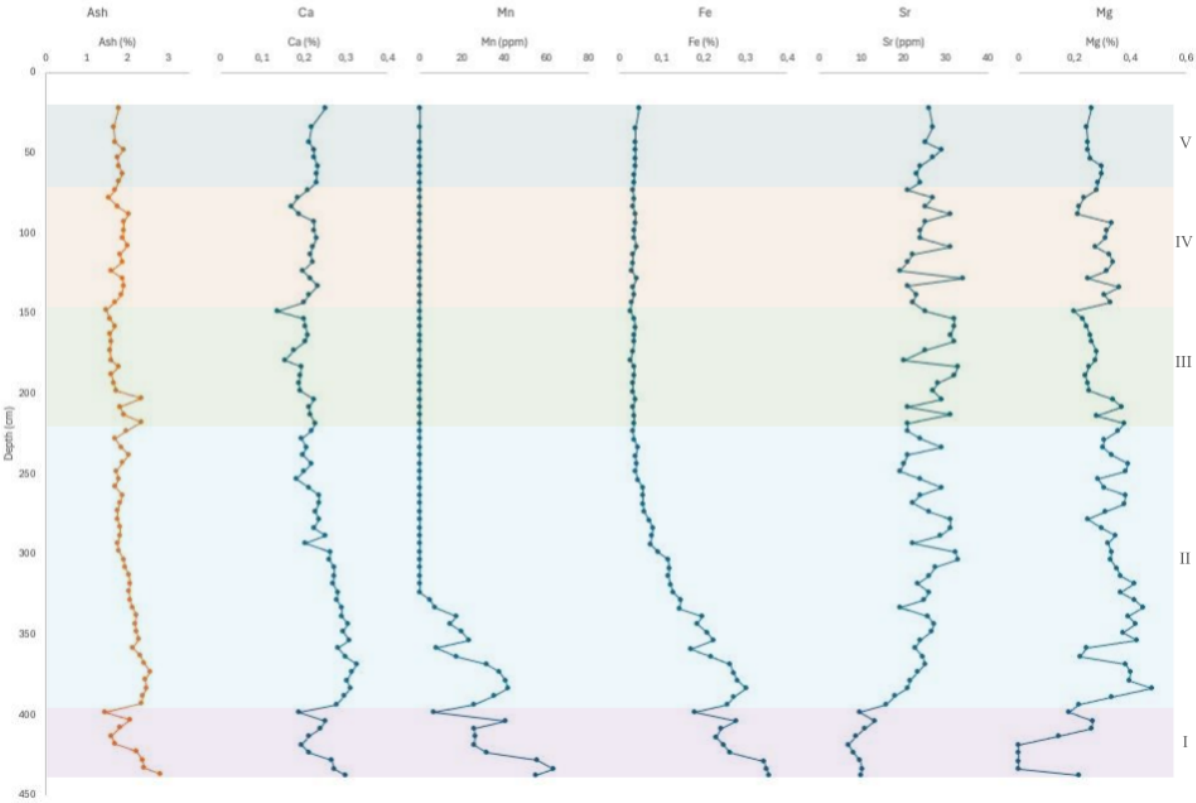


Fig. 2 – The concentration of the ash content together with the mobile elements Ca, Mn, Fe, Sr, and Mg in relation to depth. Periods I-V are indicated by the colored areas and labeled to the right.

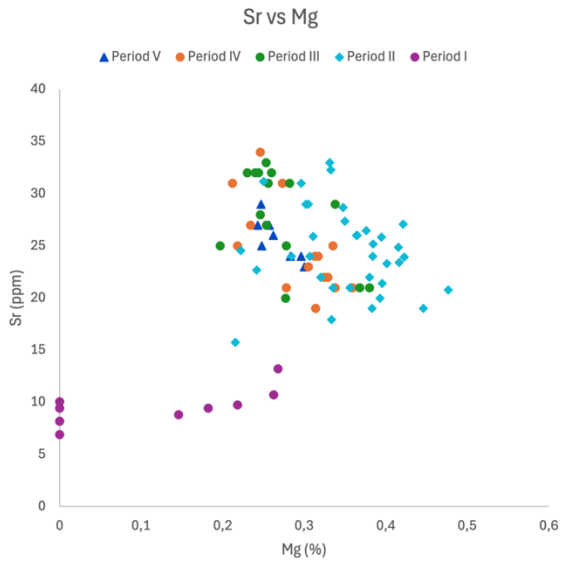


Fig. 3 – Scatterplot of Sr against Mg with period divisions.

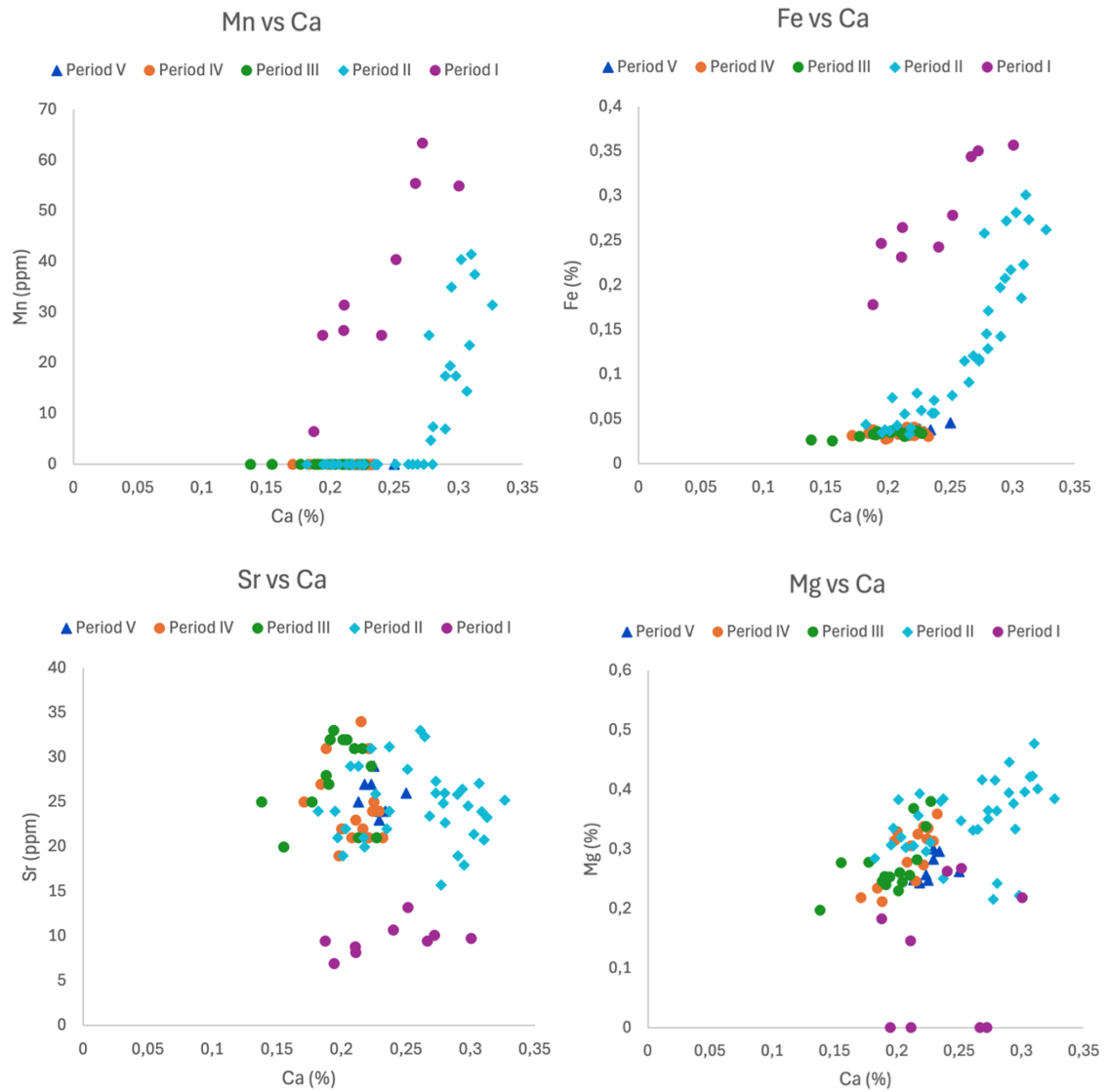


Fig. 4 – The mobile elements Mn, Fe, Sr, and Mg plotted against Ca with the five period divisions.

### 3.1.2 Trace metals

As seen in fig. 5, the trace metals do not show great variability, apart from Hg which has a peak in the oldest part of the core. Zinc, Pb, and Cu all have low concentration. Zinc has a mean value of  $1.3 \pm 0.65$  ppm (range = 0-4 ppm, n = 82), Pb has a mean value of  $0.3 \pm 0.72$  ppm (range = 0-3.5 ppm, n = 82), and Cu has a mean value of  $1.18 \pm 0.55$  ppm (range = 0-2 ppm, n = 82). The mean for Hg, including all measurements, is  $14.43 \pm 14.35$   $\mu\text{g kg}^{-1}$ , and without the oldest 20 cm where there is a clear peak, it is  $11.17 \pm 5.22$   $\mu\text{g kg}^{-1}$ . At the oldest part, the last 20 cm, the mean value is  $64.62 \pm 17.25$   $\mu\text{g kg}^{-1}$ . The lowest value for the Hg is  $3.54$   $\mu\text{g kg}^{-1}$  at 329-328 cm depth, and the highest value is  $89.07$   $\mu\text{g kg}^{-1}$  at 429-428 cm depth.

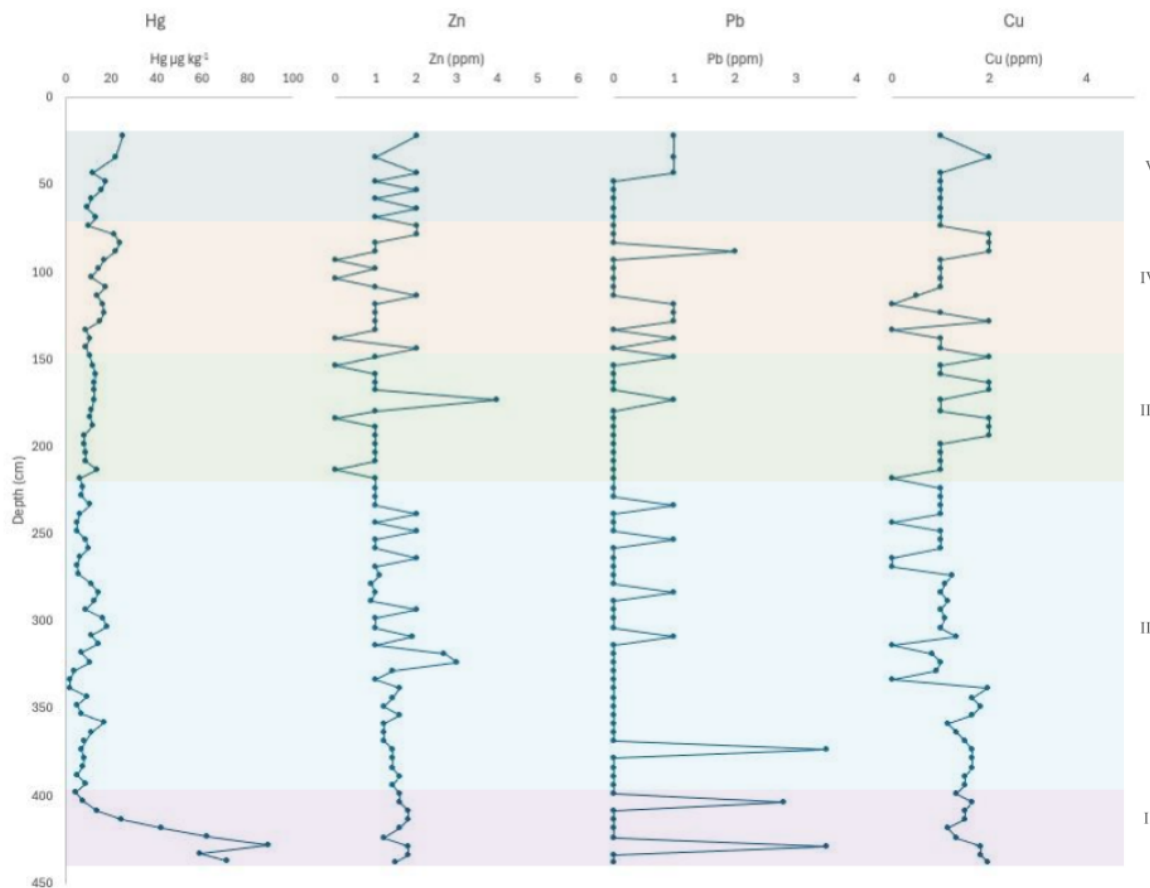


Fig. 5 – Graphs of the pollution-classified elements Hg, Zn, Pb, and Cu. Mercury is shown in  $\mu\text{g kg}^{-1}$  and the other elements are shown in ppm. The y-axis shows depth in cm. The colored areas, numbered to the right, indicate the five periods.

### 3.1.3 Lithogenic elements

Presented in fig. 6 are the lithogenic elements beside ash and wet bulk density for comparison. The gray lines labelled a-k are the dust events which will be discussed in the section 4 below. Both K and Si came out below the LOD with the S1 Titan and their graphs are therefore cut off

below 334 cm. The mean values are  $0.03 \pm 0.02\%$  for Al (range = 0-0.11%, n = 82),  $0.01 \pm 0.002\%$  for K (range = 0.007-0.017%, n = 61),  $0.04 \pm 0.02\%$  for Si (range = 0.013-0.133%, n = 61), and  $52.43 \pm 31.27$  ppm for Ti (range = 16-159 ppm, n = 82). The minimum values for each of the elements are found in Period II. However, the minimum value for K (0.007%) also shows up once in Period V. The maximum value for Al is found in the oldest sample at 438-437 cm, while the rest of the elements see their maximum values in period IV. For Ti, however, there is a close second in the oldest sample at a value of 154.43 ppm.

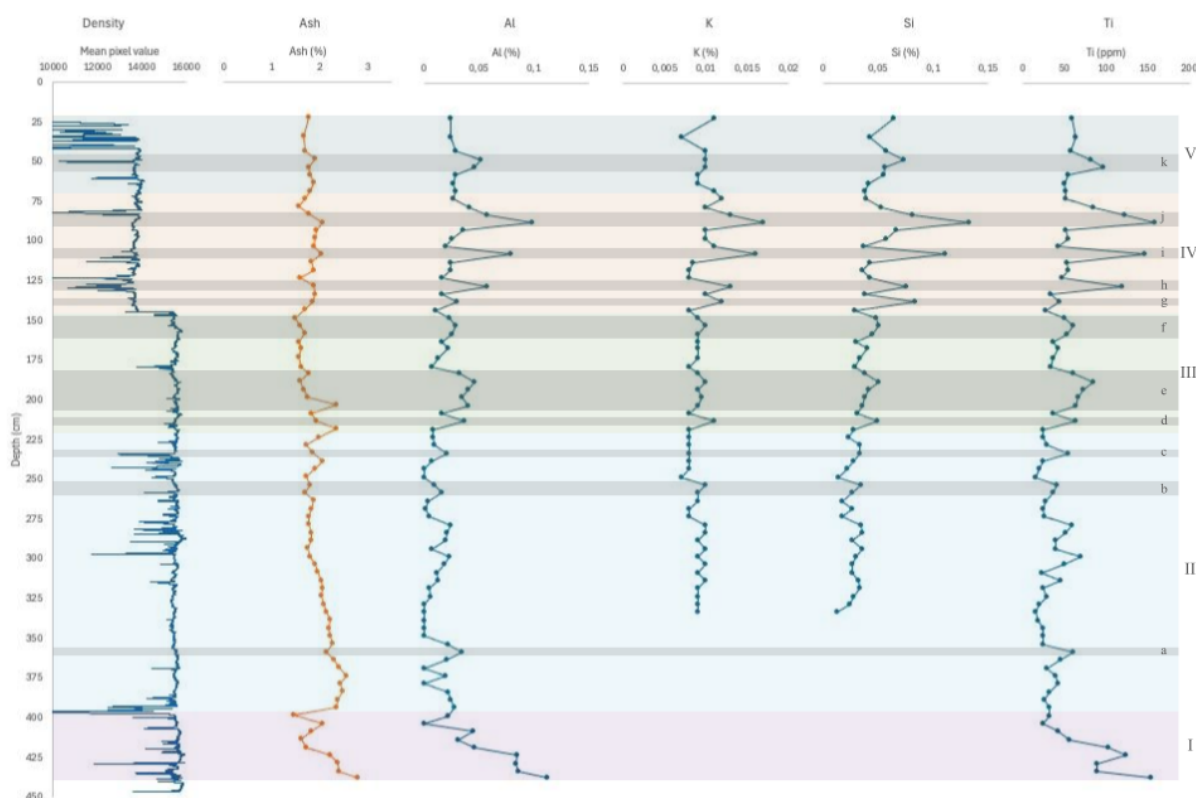


Fig. 6 – Wet bulk density, ash, and the lithogenic elements Al, K, Si, and Ti all plotted against depth. The colored areas mark the defined Periods I to V. The gray lines, labelled a-k on the right-hand side, all mark dust events.

In the scatterplots in fig. 7 the elements K, Si, and Ti are all plotted against Al. For fig. 7A-C the measurements have been divided based on the periods and in fig. 7D-F, the  $R^2$  value is annotated. The elements plot along a general line and the  $R^2$  values are high (K vs Al =  $\sim 0.62$ , Si vs Al =  $\sim 0.8$ , Ti vs Al =  $\sim 0.84$ ). In all plots we can see that Period II has the overall lowest values while Period III starts climbing upwards along the trend line. Period V overlaps Period III in biplot space. Period IV shows the most anomalous values with several points showing higher concentrations for both elements. The Ti plot is the only of the three which includes the oldest period, and here we can see that it plots all along the trend line.

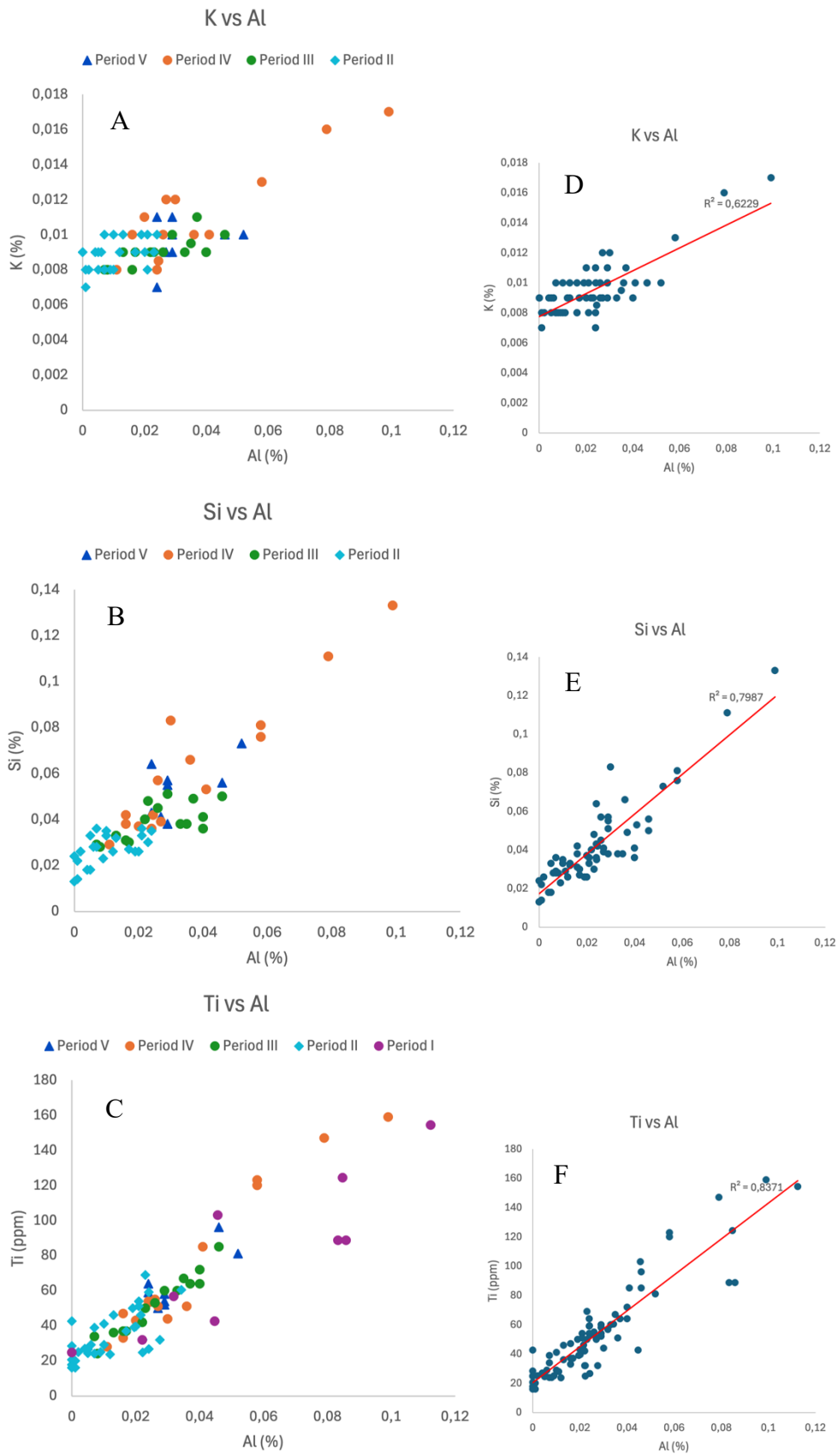


Fig. 7 – A-C: scatterplots of K, Si, and Ti against Al with period divisions, see legend. D-F: Their respective  $R^2$  values.

### 3.1.5 Chlorine

There is a high concentration of Cl throughout the sequence (fig. 8) with generally increasing amounts from the bottom and up to the maxima of 1039 ppm at 89-88 cm. After the maxima, the concentrations start somewhat decreasing again. The mean is  $569 \pm 173.53$  ppm ( $n = 82$ ) with a minimum of 281 ppm at 404-403 cm.

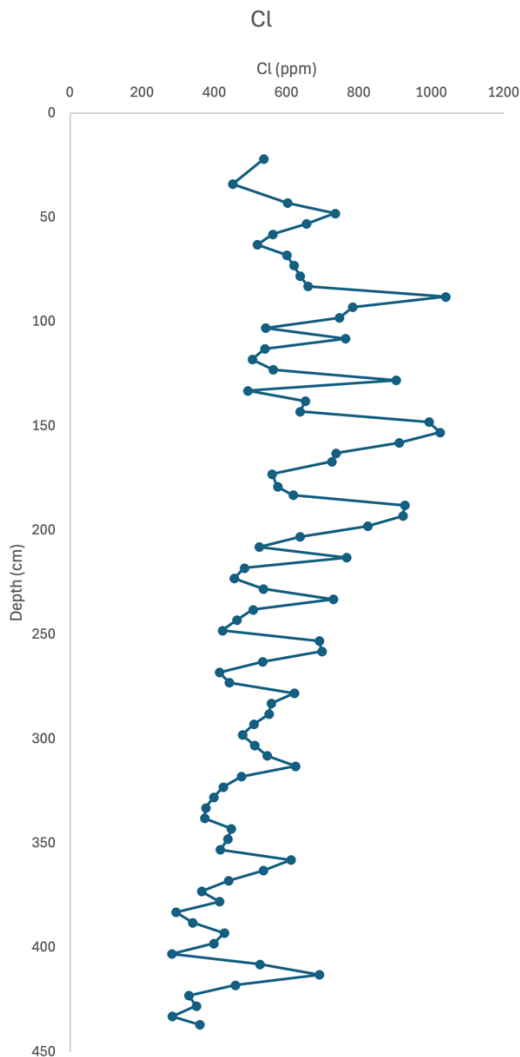


Fig. 8 – Graph of Cl in relation to depth.

### 3.2 Ash

The ash content shows moderate visual agreement with the lithogenic elements (fig. 6). While some lithogenic peaks have no respective ash peak, others have clear counterparts in the ash content. In Period I and the first half of Period II, the ash agrees rather closely with the mobile elements (fig. 2), but later they do not display the same level of similarities. The mean ash concentration is  $1.92 \pm 0.28\%$ , with a minimum of 1.46% at 399-398 cm depth and a maximum of 2.8% at 438-437 cm depth.

### 3.3 CT data

The CT data (fig. 6) is presented based on mean pixel value, a proxy for relative density. The full sequence from 438-22 cm has an average mean pixel value of  $14\,685 \pm 1\,743$ . However, as clearly visible in the graph, there is a sudden lowering of the relative density at the transition from Period III to IV. On both sides of the boundary, the density is relatively even with only minor variations. In the Periods I-III the average mean pixel value is  $15\,418 \pm 563$ , and in the Periods IV-V the average mean pixel value is  $12\,920 \pm 2\,279$ .

## 4 Discussion

### 4.1 Elemental behavior

#### 4.1.1 Mobile elements

Calcium, Mn, and Fe all show similar curves with generally decreasing concentrations between the bottom of the sequence up to approximately 273 cm, and low concentrations above this. Both Fe and Mn have been shown to be very mobile in peat (Novak et al., 2011), so the higher amounts further down in the sequence strongly suggest influence from the local water table.

Strontium and Mg have curves somewhat resembling those of the lithogenic elements rather than the mobile elements. They show inverted trends to the other mobile elements with a general increasing trend from the bottom up to ca 383 cm and higher concentrations in the shallower parts of the sequence. The reason for the relatively high concentrations of Sr and Mg compared to Ca, Fe, and Mn above 383 cm may be that the atmospheric input comes from a somewhat Mg and Sr rich source, or for the Mg may be due to influence of saltwater spray which would successively add Mg to the surface of the bog, causing the increased concentrations (REF). The scatterplot of Sr vs Mg (fig. 3) speaks to the two elements being closely linked and having a common source as most of the datapoints are gathered. Only in Period I do we see some anomalously low concentrations, mainly of Mg but also somewhat of Sr, otherwise the relatively high concentrations further up in the sequence are reflected in Period II-V.

#### 4.1.2 Trace metals

We expect trace metals such as Cu, Zn, and Pb to be immobile in the profile (Novak et al., 2011) and it is likely that these elements would be sourced from atmospheric emissions from

metallurgy. These elements show very low concentrations throughout the sequence, often below detection limit, and no major peaks of interest.

The Hg data is of interest with its maxima at 429-428 cm depth. The Hg curve resembles the curves of the redox sensitive mobile elements Mn, Fe, and to some extent Ca, as well as the lithogenic Al and Si, which all also experience a peak in concentration near the oldest part of the core. The similarity to the mobile elements indicates that the Hg may also act mobile in the bog.

#### 4.1.3 Lithogenic elements

Aluminum and Ti act conservative in the bog, as seen by their similar curves and strong display of correlation ( $R^2 \approx 0.84$  (fig. 7C)). Apart from these we can infer that Si also acts conservatively, as the available data shows a high degree of correlation between Al and Si ( $R^2 \approx 0.8$  (fig. 7B)). For K, like Si, we only have the WDXRF data, but as this data shows good correlation with Al ( $R^2 \approx 0.62$  (fig. 7A)) it can be said that K is likely conservative but may potentially be affected by another factor as well. For the present thesis, K is considered to act as a conservative element due to its curve similarity to the other lithogenic elements coupled with its good correlation with Al, but caution is taken as to not solely rely on it for any decisive conclusions.

The concentrations of the conservative elements are controlled by mineral dust input (REF). The scatterplots (fig. 7) show that these elements plot along a mixing line. This points to two main sources of mineral dust being present and mixing at certain conditions. More discussion on what this means in terms of dry periods or increased storminess below in section 4.4.

## 4.2 Deposit formation and characterization

The relatively high ash content together with Fe in the lowermost part of the sequence closely resembles the Sjöström et al. (2022) description of the south-west Sweden bog Davidsmosse (*mosse* means bog in English) and may indicate mire initiation by soil paludification, This is then followed by lower ash and Fe contents, further resembling the Davidsmosse trend and it is therefore likely that Sellevollmyra experienced a similar early history of transitioning into minerotrophic fen conditions (influence from flowing water) and later, for Sellevollmyra at around 354-323 cm, into ombrotrophic peat conditions with *Sphagnum* as the dominating species. These observations are further strengthened when comparing to Vorren et al. (2007) who noted that a change from a Cyperaceae dominated peat to a *Sphagnum*-Ericales-peat

happened at about 420 cm depth. The transition into ombrotrophic character means the bog was no longer supplied with material from flowing water and is therefore above approximately 350 cm depth a reliable source of atmospheric signals.

The very low ash content throughout the sequence is typical of an ombrotrophic peat bog (Weiss et al., 2002) and the slightly higher ash content in the bottom of the sequence points to a higher influx of minerogenic material at the start of formation, indicative of soil paludification (Sjöström et al., 2022). Worth noting is that the ash content, along with the mobile elements, decrease temporarily between ca 418 cm and 398 cm, pointing to a fairly close relation between amount of ash and mobile elements present and to a disturbance, possibly post deposition, of the early formed peat.

#### *4.2.1 Bog hydrology*

Damman (1978) looked at Traneröds mosse (the Traneröd Bog) in southern Sweden and saw similar Ca, Fe, and Mn trends at the base of their profile as at Sellevollmyra. He hypothesized that it was due to soligenous water, which is rich in these elements, influencing the bottom of the deposit as the water table rose due to increasing bog thickness. Soligenous water influence would mean we are in the fen part of the sequence and this hypothesis connects well with Sjöström et al. (2022) as discussed above. Once the influence from the soligenous water ceases we are in the bog part of the sequence.

Damman (1978) found Mg to follow the other mobile elements up to 4 m depth whereas the data for Sellevollmyra shows the opposite at approximately the same depth. Sjöström et al. (2022) also saw relatively high amounts of Mg in the bottommost part of their sequence, and it is part of their reasoning for the soil paludification start of the bog. Why Sellevollmyra shows a differing Mg concentration can be hard to say because the change of instruments mid-analysis must be considered. Between the depths at which Mg shows the somewhat anomalous trend is where the S1 Titan (EDXRF) was used. Even with corrections there is the possibility of data errors, so the dissonance between the behavior of the same element in similar types of environments may not necessarily be real. Although, when considering Damman's (1978) hypothesis, it may simply be because the soligenous water in the area had generally lower amounts of Mg compared to what is usually expected. One could speculate that the bedrock at Andøya does not contain as much Mg as in the cases of Damman (1978) and Sjöström et al. (2022) and is therefore not contributing a lot of Mg to the bog.

Up to 398 cm where we see the relatively steep decrease in most of the mobile elements, there are quite a few local maxima and minima, and this behavior may be understood

with a combination of the Sjöström et al. (2021) and Damman (1978) explanations. Initial high contents of mobile elements due to mire initiating soil paludification may be disturbed by a changing water table, leaching elements from one part and enriching another during oscillation.

### **4.3 Pollution Signals**

Based on the data of Cu, Zn, and Pb it seems that the Sellevollmyra area has not experienced a significant amount of anthropogenic pollution. This is interesting as we see pollution signals from Roman mining in Greenland ice cores (McConnell et al., 2018), meaning the aerosols from mining activities in Europe during the Roman period did travel far northward. Why Sellevollmyra does not show the same signal is likely due to the difference in sensitivity of the instruments. In McConnell et al. (2018), Pb was presented in  $\text{pg g}^{-1}$  with a range of  $\sim 1\text{-}15.5 \text{ pg g}^{-1}$ , whereas the S8 Tiger measured in ppm. In other words, it is likely that the Pb concentration was simply below LOD for the S8 Tiger and that is why we do not see similar signals to the Greenland ice cores.

The Hg data is in contrast to studies from south-west Europe where Hg accumulation rates were shown to have increased by a factor of  $3\pm 1$  from 8000 BCE until the preindustrial era (Enrico et al., 2017). It is therefore likely that the initial relatively higher concentrations of Hg are due to the difference in conditions at the start of bog formation rather than because of anthropogenic activity. Binding of Hg to ligands may affect its mobility (Schuster, 1991). Schuster (1991) explained that high concentrations of  $\text{Cl}^-$  can cause complete mobilization of Hg. As Sellevollmyra is located on the coast and shows high concentrations of Cl through the whole sequence (fig. 8), it is not unlikely that this has affected the mobility of the Hg and could be part of the reason why we see such low concentrations above 404 cm. In other words, the Hg is not a reliable signal of atmospheric pollution at Sellevollmyra.

### **4.4 Dust events**

The data for Al, K, Si, and Ti all follow each other closely and peak at the same depths (fig. 6). As mentioned previously, five periods were defined based on similarities in elemental behavior. These are: Period I: 438-398 cm, Period II: 394-223 cm, Period III: 219-148 cm, Period IV: 144-73 cm, and Period V: 69-22 cm. Dust events are indicated as: a: 359-358 cm, b: 259-253 cm, c: 234-233 cm, d: 214-213 cm, e: 204-183 cm, f: 159-148 cm, g: 139-138 cm, h: 129-128 cm, i: 109-108 cm, j: 89-83 cm, and k: 54-48 cm (fig. 6). It must be mentioned, however, that mineral dust element enrichments could also be caused by lowered peat accumulation rates (PARs) (Weiss et al., 2002), and this aspect will be discussed as well.

In the scatterplots of the lithogenic elements (fig. 7) the periods, excluding Period I, show trends of climbing along the mixing line, mentioned in 4.1.3. This indicates a general increasing importance of the second dust source as we get further up in the sequence. Period IV shows some anomalously high values and is therefore the most prominent period of mixing with a second source. However, we see the generally increasing importance of the second dust source through Period II generally plotting lower along the mixing line and Period III climbing higher, followed also by Period V which plots close to Period III, but still generally slightly further up along the mixing line. Changes in the concentrations of the lithogenic elements is caused by a change in the source of the mineral material, itself driven by shifts in vegetation or hydrology or by changes in atmospheric circulation, either as a shift in wind directions or a change in wind strengths.

In general, it would be assumed that dust events are linked to drier periods, but determination of dry shifts in a peat bog may be made through a multitude of methods. Degree of humification is often used as we would expect less decomposition during wetter periods when the peat can experience anoxic conditions due to increased water table levels, and we would expect more decomposition during drier periods when the material is exposed to a larger degree to the atmosphere. Vegetation can also be used as indicators of drier or wetter conditions as different types of plants thrive in different conditions. Humification is what was used by Vorren et al. (2007) to determine wet and dry shifts at Sellevollmyra. However, determining the degree of humification is not necessarily straightforward. Hansson et al. (2013) found that the best way to investigate decomposition, and therefore also wet and dry shifts, is to use a multiproxy approach as different proxies may show different aspects of the decay process. Here, a potential issue arises with the Vorren et al. (2007) article. They used colorimetric humification, a somewhat old-fashioned technique that is not as frequently utilized today, and von Post's humification degrees, a largely subjective field observation method. In other words, the Vorren et al. (2007) proposed wet and dry shifts serve as a good guideline, but other dry period indications such as vegetation type (Vorren et al., 2007) and wet density (present thesis) will be taken into consideration when trying to correlate the potential dust events to the conditions of the bog during the same time.

#### *4.4.1 Period I: 438-398 cm*

This period sees initial high concentrations of the lithogenic elements, most of the mobile elements, ash content, and the generally highest bulk density. As discussed earlier, the high concentrations of elements are most likely connected to conditions at the start of bog formation

and not an indicator of dust events. The relatively high wet bulk density is also not necessarily a sign of dry conditions. The very high concentration of pollen (Vorren et al., 2007) at the time indicates that the bog formed while exposed to the atmosphere, likely leading to a high degree of humification which would also contribute to the higher bulk density. The PAR was very slow (Vorren et al., 2007), enabling further enrichment of elements (Weiss et al., 2002). The end of the section is marked by a low in all mobile elements and ash content and at the same time we see a drop in density. In short, the start of the bog cannot be used to determine past dust events and storminess due to many different factors potentially influencing element concentrations as well as wet bulk density.

#### *4.4.2 Period II: 394-223 cm*

This period shows the start of lower and more gently oscillating lithogenic element concentrations. In terms of dust events, there is one possible event at 359-358 cm (a, fig. 6) where we see a moderate peak in the available mineral dust elements. According to Vorren et al. (2007), this proposed event occurred during a dry shift while the PAR was low. Both of these data support that the event likely occurred due to relatively dry conditions.

Another event is present at 259-253 cm (b, fig. 6) where we see a small peak in all of the mineral dust elements. It coincides with the end of a dry shift while the PAR was moderate (Vorren et al., 2007). This makes it likely that the mineral dust element enrichment was caused by drier conditions.

The last dust event of the period occurs at 234-233 cm (c, fig. 6). It is a minor event which is visible in the Al and Ti, with a slight general increase in the Si. This event occurred just after a dry shift, meaning there were prevailing drier conditions at the time and the PAR was still moderate (Vorren et al., 2007). In other words, no other factors seem to have played a role in the mineral dust enrichment, pointing to it being caused by dry conditions.

#### *4.4.3 Period III: 219-148 cm*

This section starts with a small peak in ash concentration which is followed closely by a small peak in the mineral dust elements. The mineral dust peak at 214-213 cm (d, fig. 6) coincides with the very end of a wet shift according to Vorren et al. (2007). However, this wet shift is closely followed by a dry shift. Considering that there will be discrepancies between the two studies, it is possible that the mineral dust enrichment is connected to the Vorren et al. (2007) dry shift rather than the wet shift. Another factor that speaks to this is the vegetation. The amount of *Calluna*, a plant that likes drier conditions, increases just before we see the peak in

the mineral dusts. The PAR is also relatively fast at this time, so the enrichment is not likely due to slow material accumulation and more likely due to an actual dust event caused by a dry shift.

The next dust event is seen between 204 and 183 cm (e, fig. 6). This event is marked by an initial increase in ash contents and generally higher mineral dust element concentrations. As opposed to the previous dust events, this one is slightly prolonged and is most likely the result of generally increased atmospheric input. When comparing with Vorren et al. (2007), we see that the dust event starts during a wet shift but spans over a full dry shift and wet shift as well. This is where one can be critical of the Vorren et al. (2007) methods for determining humification. In Table 2 in Vorren et al. (2007), the period during which this dust event likely took place starts at 5 humification degrees, goes into 3-4 humification degrees, and ends at 5-6 humification degrees on von Post's scale. These shifts do not perfectly align with the supposed wet and dry shifts as seen in Table 3. It is possible that there were wetter conditions at this time, and if so, the dust event would likely have been caused by increased storminess rather than by dry conditions. However, with criticism towards Vorren et al.'s (2007) methods, the wet and dry shifts may not be entirely accurate, so at least some of the mineral dust enrichment we see could also be caused by some relatively drier conditions.

At 159-148 cm (f, fig. 6) there is another period of increased atmospheric input as we clearly see higher levels of Si and Ti, and somewhat higher levels of Al and K. Vorren et al. (2007) indicate largely wet conditions both before and after the mineral dust peak. However, something that would speak against wetter conditions is a fairly sudden increase in *Calluna* which would potentially indicate drier conditions, and the PAR remains relatively fast. The cause for the dust event is therefore not certain as it could be both due to drier conditions and due to increased storminess.

#### 4.4.4 Period IV: 144-73 cm

The start of this section sees a sudden decrease in density. As Vorren et al. (2007) recorded, Sellevollmyra saw a hiatus between ca 1000-500 BCE, likely due to much drier conditions, fires, or human impact. The combined dust events of Period IV overlap with this hiatus, so the increased atmospheric input over the period was interrupted at some point or another, but it will be handled as one continuous section for the present thesis. During this period, we see four major peaks in the concentration of the mineral dust elements. Based on the mineral dust element graphs, the individual dust events occurred at 139-138 cm (g, fig. 6), 129-128 cm (h, fig. 6), 109-108 cm (i, fig. 6), and 89-83 cm (j, fig. 6). Apart from 139-138 cm, the rest of the

events either coincide with dry shifts or are close to dry periods. Since the 139-138 cm peak is the least prominent of the four, it is likely that the conditions were wetter, but that increased storminess prevailed and causes the peak we are seeing. For the rest of the peaks, it is likely that these were caused by a combination of dry conditions and increased storminess as they are very prominent. In the scatter plots (fig. 7) we see large influence from the second dust source as mentioned in 4.1.3 since the dust events plot further along the mixing line than the dust events of other periods. This supports increased storminess as it would enable dust from more distal sources. Sjögren (2009) studied SARs a bit north of Sellevollmyra. In this study, northern Norway was shown to have increased sand accumulation from 500 BCE toward 1 BCE. This timespan coincides well with the later two of the four dust events, further supporting the likelihood of increased storminess in this period.

In the Ti vs Al plot (fig. 7) where we have data for the bottommost part of the sequence, we also see similarities between period IV and the start of bog formation. This shows that the mixing of the sources gives a geochemistry similar to that of the soligenous water, and therefore also bedrock, at Sellevollmyra.

#### 4.2.5 Period V: 69-22cm

This section shows one potential dust event at 54-48 cm (k, fig. 6). Here we see a slight increase in ash and distinct peaks in three of the lithogenic elements, Al, Si, and Ti. There is a definite increase in amount of *Calluna* seen in the profile and the event overlaps a supposed dry shift at 50-48 cm (Vorren et al., 2007). When comparing with Vorren et al. (2007), the dust event is seen to probably occur just after 500 CE, a time when Sjögren (2009) found increased sand accumulation. This is in support of the dust event occurring, at least partly, due to increased storminess and the larger amount of *Calluna* and the potential dry shift indicates that it was likely a relatively drier period as well.

After the 54-48 cm event there are no other indications of any more dust events. There is some degree of variability in the topmost samples but no obvious general peaks. Worth mentioning is that the profile of the present thesis ends at 22 cm depth, making it possible that records of increased atmospheric input in recent years is lost.

## 5 Conclusions

- (i) Calcium, Mn, and Fe were shown to be highly mobile in the profile. Strontium and Mg show more similarities to the lithogenic elements than the mobile elements and

are concluded to be derived from a Sr and Mg rich mineral dust source or, in the case of Mg, potentially from the proximity to the ocean. Copper, Zn, and Pb are assumed to be immobile in the bog (Novak et al., 2011) and show low concentrations throughout the sequence. Mercury was concluded to behave as a mobile element. The lithogenic elements were shown to be conservative and derived from mineral dust.

- (ii) The bog at Sellevollmyra was likely formed through soil paludification, followed by a transition into minerotrophic fen conditions and later ombrotrophic bog conditions. This is supported by similarities in the oldest part of the sequence to the Sjöström et al. (2022) profile and by comparisons with the Vorren et al. (2007) study.
- (iii) Based on our results, Sellevollmyra has generally seen low amounts of pollution. However, potential similarities to the Greenland ice cores have likely been lost due to differing instrument sensitivity, and it therefore remains uncertain whether or not the two areas have experienced the same kind and amount of pollution. To find certainty, further studies would have to be made using a more sensitive instrument to measure the true concentration of Pb in the sequence.
- (iv) It is concluded that the Sellevollmyra area has experienced eleven events of increased atmospheric input, and after thorough comparisons and connections with Vorren et al. (2007), as well as Sjögren (2008) for the most recent 3000 years, they have been shown to be caused by increased storminess, drier periods, or a combination of the two. The dust events occurred at 359-358 cm, 259-253 cm, 234-233 cm, 214-213 cm, 204-183 cm, 159-148 cm, 139-138 cm, 129-128 cm, 109-108 cm, 89-83 cm, and 54-48 cm.

For future studies it is encouraged to measure grain amounts and sizes to further investigate the strengths and frequencies of storms and dust events. This is to keep building on the thorough Vorren et al. (2007) study, as well as the Sjögren (2008) record of storminess in northern Norway, to create an archive which stretches even further back in history. It would also be interesting to see more peat bog mineral dust studies from arctic sites to further build on our understanding of the atmospheric patterns and global distribution of airborne material.

## **Acknowledgements**

First, I would like to thank my supervisor, Malin Kylander, for her invaluable guidance throughout the whole project, helping me structure my thoughts and see the bigger picture when I was feeling lost. Ylva Palmgren is thanked for the work she did on the cores prior to the start of my project, such as the actual sampling and the CT-scanning, as well as for helping me with the C<sup>14</sup> picking and understanding my data. I would also like to thank Johan Rydberg for welcoming me to Umeå and helping me carry out the XRF analysis. Last but not least, I would like to acknowledge everyone at the institution who helped me throughout my project, with freeze drying, milling, Hg-analysis, and more, and who made me feel like I was welcome and a true part of the team.

## Sources

**Albani, S., Mahowald, N.M., Winckler, G., Anderson, R.F., Bradtmiller, L.I., Delmonte, B., François, R., Goman, M., Heavens, N.G., Hesse, P.P., Hovan, S.A., Kang, S.G., Kohfeld, K.E., Lu, H., Maggi, V., Mason, J.A., Mayewski, P.A., McGee, D., Miao, X., Otto-Bliesner, B.L., Perry, A.T., Pourmand, A., Roberts, H.M., Rosenbloom, N., Stevens, T. and Sun, J.** (2015) 'Twelve thousand years of dust: the Holocene global dust cycle constrained by natural archives', *Climate of the Past*, 11(6), pp. 869–903.

**Blackford, J.** (2000) 'Paleoclimatic records from peat bogs', *Trends in Ecology & Evolution*, 15(5), pp. 193–198.

**Boyer, A., Ning, P., Killely, D., Klukas, M., Rowan, D., Simpson, A.J. and Passeport, E.** (2018) 'Strontium adsorption and desorption in wetlands: Role of organic matter functional groups and environmental implications', *Water Research*, 133, pp. 27–36.

**Chen, L., Zhou, M., Wang, J., Zhang, Z., Duan, C., Wang, X., Zhao, S., Bai, X., Li, Z., Li, Z. and Fang, L.** (2022) 'A global meta-analysis of heavy metal(loid)s pollution in soils near copper mines: Evaluation of pollution level and probabilistic health risks', *Science of The Total Environment*, 835, pp. 1–11.

**Damman, A. W. H.** (1978) 'Distribution and movement of elements in ombrotrophic peat bogs', *Oikos*, 30, pp. 480–495.

**De Vleeschouwer, F., Le Roux, G. and Shotyk, W.** (2010) 'Peat as an archive of atmospheric pollution and environmental change: A case study of lead in Europe', *PAGES*, 18(1), pp. 20–22.

**Enrico, M., Le Roux, G., Heimbürger, L-E., Van Beek, P., Souhaut, M., Chmeleff, J. and Sonke, J.E.** (2017) 'Holocene Atmospheric Mercury Levels Reconstructed from Peat Bog Mercury Stable Isotopes', *Environmental Science & Technology*, 51(11), pp. 5899–5906.

**Gorham, E. and Janssens, J.A.** (2005) 'The distribution and accumulation of chemical elements in five peat cores from the mid-continent to the eastern coast of North America', *Wetlands*, 25, pp. 259–278.

**Hansson, S.V., Bindler, R. and De Vleeschouwer, F.** (2015) 'Using Peat Records as Natural Archives of Past Atmospheric Metal Deposition', in Blais, J.M., Rosen, M.R. and Smol, J.P. (eds.) *Environmental Contaminants*. Vol. 18. Dordrecht: Springer Science+Business Media, pp. 323–354.

**Hansson, S.V., Rydberg, J., Kylander, M., Gallagher, K. and Bindler, R.** (2013) 'Evaluating paleoproxies for peat decomposition and their relationship to peat geochemistry', *The Holocene*, 23(12), pp. 1666–1671.

**Hylander, L.D. and Goodsite, M.E.** (2006) 'Environmental costs of mercury pollution', *Science of The Total Environment*, 368(1), pp. 352–370.

**Johnson, R.G. and King, B.-S.L.** (1987) 'Energy-Dispersive X-ray Fluorescence Spectrometry', in Baedecker, P.A. (ed.) *Methods for Geochemical Analysis*. Washington, D.C.: United States Government Printing Office (USGS Bulletin 1770, Section F1).

**Jones, J. M. and Hao, J.** (1993) 'Ombrotrophic peat as a medium for historical monitoring of heavy metal pollution', *Environmental Geochemistry and Health*, 15, pp. 67–74.

**Kao, R.T., Dault, S. and Pichay, T.** (2004) 'Understanding the Mercury Reduction Issue: The Impact of Mercury on the Environment and Human Health', *Journal of the California Dental Association*, 32(7), pp. 574–579.

**Kirchhefer, A.J.** (2001) 'Reconstruction of summer temperatures from tree-rings of Scots pine (*Pinussylvestris* L.) in coastal northern Norway', *The Holocene*, 11(1), pp. 41–52.

**Knippertz, P. and Stuut, J.-B.W.** (2014) *Mineral Dust*. Dordrecht: Springer Science+Business Media. pp. 2–3.

**Kylander, M.E., Martínez-Cortizas, A., Bindler, R., Greenwood, S.L., Mörth, C.-M. and Rauch, S.** (2016) 'Potentials and problems of building detailed dust records using peat archives: An example from Store Mosse (the "Great Bog"), Sweden', *Geochimica et Cosmochimica Acta*, 190, pp. 156–174.

**Kylander, M.E., Martínez-Cortizas, A., Bindler, R., Kaal, J., Sjöström, J.K., Hansson, S.V., Silva-Sánchez, N., Greenwood, S.L., Gallagher, K., Rydberg, J., Mörth, C.-M. and Rauch, S.** (2018) 'Mineral dust as a driver of carbon accumulation in northern latitudes', *Scientific Reports*, 8(6876), pp. 1–10.

**Lavoie, M., Paré, D., Fenton, N., Groot, A. and Taylor, K.** (2005) 'Paludification and management of forested peatlands in Canada: a literature review', *Environmental Reviews*, 13(2), pp. 21–50.

**Mandal, G., Mandal (Nandi), A. and Chakraborty, A.** (2022) 'The toxic effect of lead on human health', *Human Biology and Public Health*, 3, pp. 1–11.

**Martínez Cortizas, A., García-Rodeja Gayoso, E. and Weiss, D.** (2002) 'Peat bog archives of atmospheric metal deposition', *Science of The Total Environment*, 292(1–2), pp. 1–5.

**McConnell, J.R., Wilson, A.I., Stohl, A., Arienzo, M.M., Chellman, N.J., Eckhardt, S., Thompson, E.M., Pollard, A.M. and Steffensen, J.P.** (2018) 'Lead pollution recorded in Greenland ice indicates European emissions tracked plagues, wars, and imperial expansion during antiquity', *PNAS*, 115(22), pp. 5726–5731.

**Meena, V., Dotaniya, M.L., Saha, J.K., Das, H. and Patra, A.K.** (2019) 'Impact of Lead Contamination on Agroecosystem and Human Health', in Gupta, D.K., Chatterjee, S. and Walther, C. (eds.) *Lead in Plants and the Environment*. Cham: Springer, pp. 67–82.

**Novak, M. and Pacherova, P.** (2008) 'Mobility of trace metals in pore waters of two Central European peat bogs', *Science of The Total Environment*, 394(2–3), pp. 331–337.

**Novak, M., Zemanova, L., Voldrichova, P., Stepanova, M., Adamova, M., Pacherova, P., Komarek, A., Krachler, M. and Prechova, E.** (2011) 'Experimental Evidence for Mobility/Immobilty of Metals in Peat', *Environmental Science & Technology*, 45(17), pp. 7180–7187.

**Odukoya, O.O., Arowolo, T.A. and Bamgbose, O.** (2000) 'Pb, Zn, and Cu levels in tree barks as indicator of atmospheric pollution', *Environment International*, 26(1–2), pp. 11–16.

**Olesen, O., Lundin, E., Nordgulen, Ø., Osmundsen, P.T., Skilbrei, J.R., Smethurst, M.A., Solli, A., Bugge, T. and Fichler, C.** (2002) 'Bridging the gap between the onshore and offshore geology in Nordland, northern Norway', *Norwegian Journal of Geology*, 82, pp. 243–262.

**Olsen, L., Sveian, H., Ottesen, D. and Rise, L.** (2013) 'Quaternary glacial, interglacial and interstadial deposits of Norway and adjacent onshore and offshore areas', in Olsen, L., Fredin, O. and Olesen, O. (eds.) *Quaternary Geology of Norway*, Geological Survey of Norway Special Publication, 13, pp. 79–144.

**Potts, P.J.** (1987) *Handbook of Silicate Rock Analysis*. New York: Springer Science+Business Media, pp. 226–285.

**Schaffhauser, A., Payette, S., Garneau, M. and Robert, C.É.** (2017) 'Soil paludification and *Sphagnum* bog initiation: the influence of indurated podzolic soil and fire', *Boreas*, 46(3), pp. 428–441.

**Schuster, E.** (1991) 'The behavior of mercury in the soil with special emphasis on complexation and adsorption processes - a review of the literature', *Water, Air, & Soil Pollution*, 56, pp. 667–680.

**Sjögren, P.** (2009) 'Sand mass accumulation rate as a proxy for wind regimes in the SW Barents Sea during the past 3 ka', *The Holocene*, 19(4), pp. 591–598.

**Sjöström, J.K., Bindler, R., Martínez Cortizas, Björck, S., A., Hansson, S.V., Karlsson, A., Ellerton, D.T. and Kylander, M.E.** (2022) 'Late Holocene peat paleodust deposition in south-western Sweden - exploring geochemical properties, local mineral sources and regional aeolian activity', *Chemical geology*, 602, pp. 1–14.

**Timothy, N. and Williams, E.T.** (2019) 'Environmental Pollution by Heavy Metal: An Overview', *International Journal of Environmental Chemistry*, 3(2), pp. 72–82.

**Van, H-T., Hoang, V.H., Nga, L.T.Q. and Nguyen, V.Q.** (2024) 'Effects of Zn pollution on soil: Pollution sources, impacts and solutions', *Results in Surfaces and Interfaces*, 17, pp. 1–9.

**Vorren, K.-D., Blaauw, M., Wastegård, S., van der Plicht, J. and Jensen, C.** (2007) 'High-resolution stratigraphy of the northernmost concentric raised bog in Europe: Sellevollmyra, Andøya, northern Norway', *Boreas*, 36(3), pp. 253–277.

**Weiss, D., Shotyk, W., Rieley, J., Page, S., Gloor, M., Reese, S. and Martínez-Cortizas, A.** (2002) 'The geochemistry of major and selected trace elements in a forested peat bog, Kalimantan, SE Asia, and its implications for past atmospheric dust deposition', *Geochimica et Cosmochimica Acta*, 66(13), pp. 2307–2323.